

University of Wollongong

Research Online

Faculty of Engineering and Information
Sciences - Papers: Part B

Faculty of Engineering and Information
Sciences

2019

First measurements with a plastic scintillation dosimeter at the Australian MRI-LINAC

Levi Madden

University of Wollongong, Ingham Institute for Applied Medical Research, ljm898@uowmail.edu.au

James Archer

University of Wollongong, jia335@uowmail.edu.au

Enbang Li

University of Wollongong, enbang@uow.edu.au

Urszula Jelen

Ingham Institute for Applied Medical Research

Bin Dong

Ingham Institute for Applied Medical Research

See next page for additional authors

Follow this and additional works at: <https://ro.uow.edu.au/eispapers1>



Part of the [Engineering Commons](#), and the [Science and Technology Studies Commons](#)

Recommended Citation

Madden, Levi; Archer, James; Li, Enbang; Jelen, Urszula; Dong, Bin; Roberts, Natalia; Holloway, Lois C.; and Rosenfeld, Anatoly B., "First measurements with a plastic scintillation dosimeter at the Australian MRI-LINAC" (2019). *Faculty of Engineering and Information Sciences - Papers: Part B*. 3170.
<https://ro.uow.edu.au/eispapers1/3170>

Research Online is the open access institutional repository for the University of Wollongong. For further information contact the UOW Library: research-pubs@uow.edu.au

First measurements with a plastic scintillation dosimeter at the Australian MRI-LINAC

Abstract

MRI-LINACs combine MRI and LINAC technologies with the potential for image guided radiation therapy with optimal soft-tissue contrast. In this work, we present the advantages and limitations of plastic scintillation dosimeters (PSDs) for relative dosimetry with MRI-LINACs. PSDs possess many desirable qualities, including magnetic field insensitivity and irradiation angle independence, which are expected to make them suitable for dosimetry with MRI-LINACs. An in-house PSD was used to measure field size output factors as well as a percent depth dose distribution and the beam quality index TPR_{20/10} at a [Formula: see text] cm² field size. Measurements were repeated with a Scanditronix/Wellhofer FC65-G ionisation chamber and PTW 60019 microDiamond detector for comparison. Relative differences were calculated between the three detectors, where the mean difference in dose was 1.2% between the PSD and ionisation chamber, 1.9% between the PSD and microDiamond detector and 1.3% between the microDiamond detector and the ionisation chamber. The closeness between the three mean differences in doses suggests that PSDs are feasible for relative dosimetry with MRI-LINACs.

Disciplines

Engineering | Science and Technology Studies

Publication Details

Madden, L., Archer, J., Li, E., Jelen, U., Dong, B., Roberts, N., Holloway, L. & Rosenfeld, A. (2019). First measurements with a plastic scintillation dosimeter at the Australian MRI-LINAC. *Physics in Medicine and Biology*, 64 (17), 175015-1-175015-8.

Authors

Levi Madden, James Archer, Enbang Li, Urszula Jelen, Bin Dong, Natalia Roberts, Lois C. Holloway, and Anatoly B. Rosenfeld

First measurements with a plastic scintillation dosimeter at the Australian MRI-LINAC

Levi Madden^{a,b}, James Archer^a, Enbang Li^{a,*}, Urszula Jelen^b, Bin Dong^b,
Natalia Roberts^{a,b}, Lois Holloway^b, Anatoly Rosenfeld^{a,c}

^a*Centre for Medical Radiation Physics, University of Wollongong, NSW 2522, Australia*

^b*Ingham Institute for Applied Medical Research Institute, Liverpool, NSW 2170, Australia*

^c*Illawarra Medical and Health Research Institute, University of Wollongong, NSW 2522, Australia*

Abstract

MRI-LINACs combine MRI and LINAC technologies with the potential for image guided radiation therapy with optimal soft-tissue contrast. In this work, we present the advantages and limitations of plastic scintillation dosimeters (PSDs) for relative dosimetry with MRI-LINACs. PSDs possess many desirable qualities, including magnetic field insensitivity and irradiation angle independence, which are expected to make them suitable for dosimetry with MRI-LINACs. An in-house PSD was used to measure field size output factors as well as a percent depth dose distribution and the beam quality index $\text{TPR}_{20/10}$ at a $10.5 \times 10.5 \text{ cm}^2$ field size. Measurements were repeated with a Scanditronix/Wellhofer FC65-G ionisation chamber and PTW 60019 microDiamond detector for comparison. Relative differences were calculated between the three detectors, where the mean difference in dose was 1.2% between the PSD and ionisation chamber, 1.9% between the PSD and microDiamond detector and 1.3% between the microDiamond detector and the ionisation chamber. The closeness between the three mean differences in doses suggests that plastic scintillation dosimeters are feasible for relative dosimetry with MRI-LINACs.

Keywords: MRI-LINAC, Fiber optic dosimeter, Plastic scintillator, dosimetry

*Corresponding author

Email address: enbang@uow.edu.au (Enbang Li)

1. Introduction

MRI-Linear accelerators (MRI-LINACs) combine an MRIs optimal soft-tissue contrast and a modern LINACs highly conformal dose distributions to deliver image guided radiation therapy with non-invasive tumour tracking [1]. For dosimetry with MRI-LINACs, the presence of the MRIs magnetic field alters the trajectories of charged particles traversing through the magnetic field and consequently the dose distributions delivered [2, 3, 4, 5]. The trajectory taken, and hence dose deposited by a charged particle in a volume of material is dependent on a materials density [2, 3]. Dosimeters with material densities not matching the density of water can have their accuracy compromised, however with correction they can be applied for MRI-LINAC dosimetry [6, 7]. Dosimeters that are minimally affected by magnetic fields are sought for MRI-LINAC dosimetry in conditions where the accuracy of other dosimeters may not be ensured [8, 9, 10].

Plastic scintillation dosimeters (PSDs) consist of plastic scintillator volumes coupled to optical fibers and have numerous dosimetric qualities that suggest they are viable for MRI-LINAC dosimetry. In a recent study by Therriault-Proux *et al.* [9], two PSDs were investigated to determine their magnetic field strength dependence. The PSDs responses increased by $(2.4 \pm 0.3)\%$ and $(2.4 \pm 0.1)\%$, while Monte Carlo simulations in similar irradiation conditions reported a physical dose increase of 2.2% [6]. The authors attributed the PSDs increase in response to an increase in the physical dose deposited in the PSD, rather than changes in the PSDs sensitivity [9]. PSDs have also been shown to possess many desirable qualities for dosimetry with LINACs, including water equivalence [11, 12, 13], energy independence for LINAC photon beams [14], dose rate independence (i.e. a dose rate dependence less than 1%) [14, 15, 16], irradiation angle independence [13, 14, 15], high spatial resolutions [17, 18] and real time responses [11, 19]. PSDs have been used effectively for small field dosimetry [20, 21, 22] and *in vivo* dosimetry [23, 24, 25] with clinical LINACs. Given these qualities and their non-ferromagnetic composition, PSDs are promising

prospects for MRI-LINAC dosimetry. The aim of this work was to apply and evaluate a PSD for relative dosimetry with an MRI-LINAC and present their advantages and limitations for relative dosimetry with MRI-LINACs.

2. Materials and Methods

The Australian MRI-LINAC project combines a 1 T open bore MRI scanner with a Varex Linatron-MP fitted with a Millenium 120 multileaf collimator (Varian, USA), shown in Figure 1 (a). The LINAC was calibrated to deliver a 1.033 Gy/MU dose to the MRIs isocentre at 10 cm depth, 10.5×10.5 cm² field size, and 2.469 m source-isocentre distance. For all measurements, the Varian Linatron-MP produced a 6 MV pulsed beam with frequency 200 Hz. Multileaf collimator (MLC) defined output factors were measured using an in-house plastic scintillation dosimeter, an ionisation chamber (FC65-G by Scanditronix / Wellhofer) and a PTW microDiamond type 60019 detector. The MLC defined output factors were measured at depths of 10 cm and 20 cm in Gammex RMI-457 solid water for field sizes between 2.6×2.6 cm² and 21.0×21.0 cm² with the setup shown in Figure 1 (b). A percent depth dose distribution (PDD) was measured at a field size of 10.5×10.5 cm² using all dosimeters. $\text{TPR}_{20/10}$ was measured at a field size of 10.5×10.5 cm² using the ionisation chamber and in house plastic scintillation dosimeter. To quantify the variations in the measured responses of the output factors and the PDD, each measurement was repeated 5 times with the PSD and 3 times with the ionisation chamber and microdiamond detector. To calculate the uncertainty in each mean response of output factors and PDD, the standard error of each mean response was combined with the standard error in the mean response at the reference point.

A Scanditronix/Wellhofer DOSE-1 reference class electrometer was used to measure the response of the ionisation chamber and microDiamond detector. For measurements with the PTW60019 microDiamond detector, the detector was orientated with its central axis parallel to the incident photon beam and magnetic field directions. For measurements with the ionisation chamber, the

chambers central axis was orientated perpendicular to the magnetic field direction and the direction of the incident photon beam, matching the orientation of the PSD shown in Figure 1 (b).

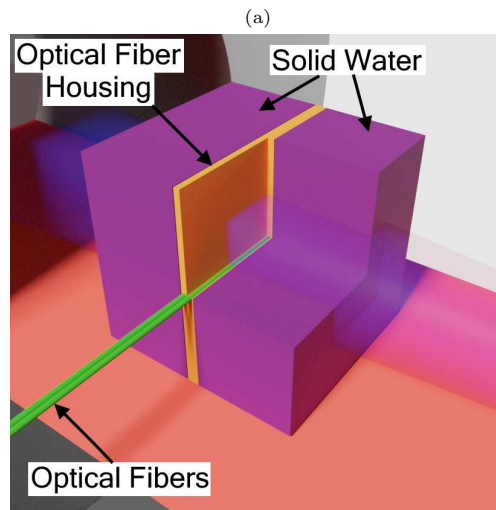
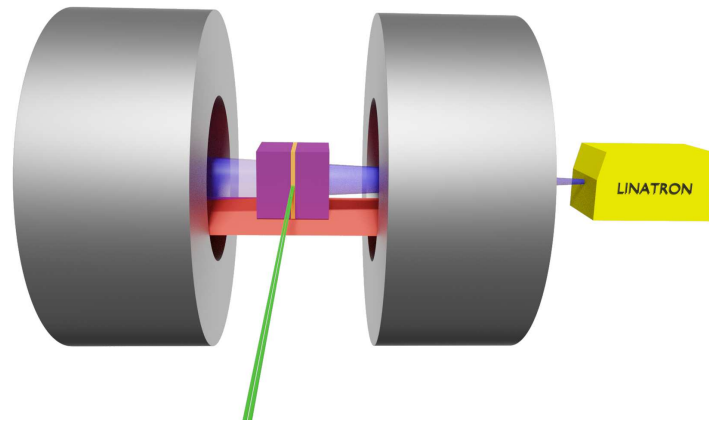


Figure 1: (a) Render of the Australian MRI-LINAC and (b) render with a cutaway to show the solid water phantom, solid water housing and PSD in the optical fiber housing in the setup used.

The plastic scintillation dosimeter consisted of a cylindrical plastic scintillator volume (BC444 by Saint Gobain) optically coupled to an Eska CK-40 optical

fiber. The BC444 volume had a length of 0.8 mm and a diameter of 2.2 mm and the optical fiber had a length of 15 m, an inner core diameter of 0.98 mm, a cladding diameter of 1 mm and a jacket diameter of 2.2 mm. To correct for Cerenkov radiation generated in the optical fiber, a secondary fiber with no scintillator was used to measure the Cerenkov radiation produced in the PSD. This is known as background subtraction, and is considered the gold-standard in the field of PSD [11, 26]. A reference probe was constructed from an Eska CK-40 optical fiber matching that of the PSD. The tips of the scintillator and reference probes were coated in black paint to prevent visible light from entering either of the probes. For measurements with the plastic scintillation dosimeter, an optical fiber housing was used to hold the scintillator and reference probes consisting of a 1 cm thick sheet of perspex with a 2.2 mm wide, 4.4 mm deep housing groove machined into the perspex, matching the housing used by Archer *et al.* [27] and Madden *et al.* [28, 29]. The housing groove was filled with ultrasound gel (Aquasonic 100 by Parker Laboratories, INC) with the PSD and reference probe placed in the housing groove to eliminate air gaps between the optical fibers and perspex in the housing groove. For measurements with the PSD, the optical fibers were orientated perpendicular to the direction of the MRI-LINACs photon beam, as shown in Figure 1 (b).

Two matching photomultiplier tubes (RCA 4526) operating in analogue mode were used to detect the optical signals generated in PSD and reference fiber. A digital oscilloscope (PicoScope PS6404D) was used to record the PSD and reference probe signals simultaneously as voltage-time waveforms, with the digital oscilloscope set to AC coupling. Waveforms recorded by the digital oscilloscope were recorded at a sampling frequency of 625 MHz for a duration of 16 μ s per waveform. Integral responses of the scintillator and reference probes were measured by delivering a fixed quantity of monitor units, recording the PMTs outputs with the digital oscilloscope when triggered and summing across all measured waveforms for the duration of the radiation deliver. Approximately 4000 treatment pulses were recorded for each PSD measurement made; a sample integral waveform (summed from the approximate 4000 treatment pulses) is

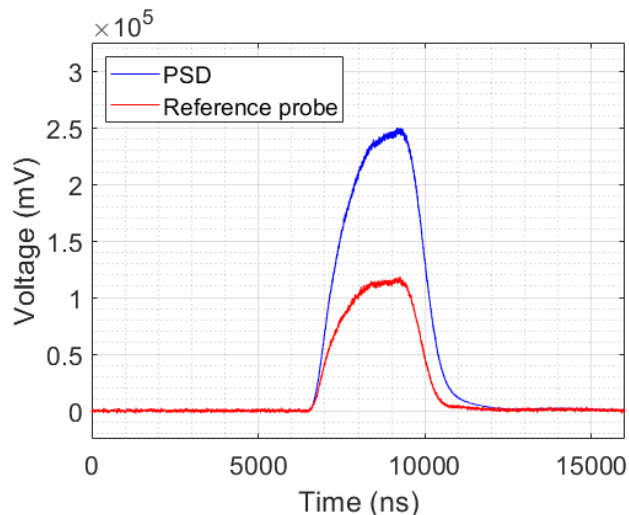


Figure 2: PSD is the signal produced by the plastic scintillation dosimeter while Reference probe is the signal produced by the reference probe. The signals presented are the integral PSD and reference probe responses (as a function of time), summed across all waveforms captured during dose delivery.

presented in Figure 2.

To achieve matching irradiation conditions between the PSD and reference probe, the reference probe and PSD were aligned tip to tip and placed against each other in the optical fiber housing. The PSD signal (scintillation and Cerenkov radiation) and reference probe signal (Cerenkov radiation only) were measured simultaneously using the two matching photomultiplier tubes. The photomultiplier tubes required cross calibration to ensure that the Cerenkov radiation measured with the reference probe for one PMT matched the Cerenkov radiation measured by the PSD for the other PMT. PMTs were cross calibrated by measuring the integral response of each fiber optic probe with each PMT, taking the ratios of each probes integral responses between PMTs and geometrically averaging these two ratios as in Archer *et al.* [27]; the resultant value was the cross calibration factor between the two PMTs. For background subtraction, the stem signal correction was performed by taking the PSD signal measured by one PMT, subtracting the reference probes signal multiplied by

the cross calibration factor and integrating this difference in signals.

3. Results

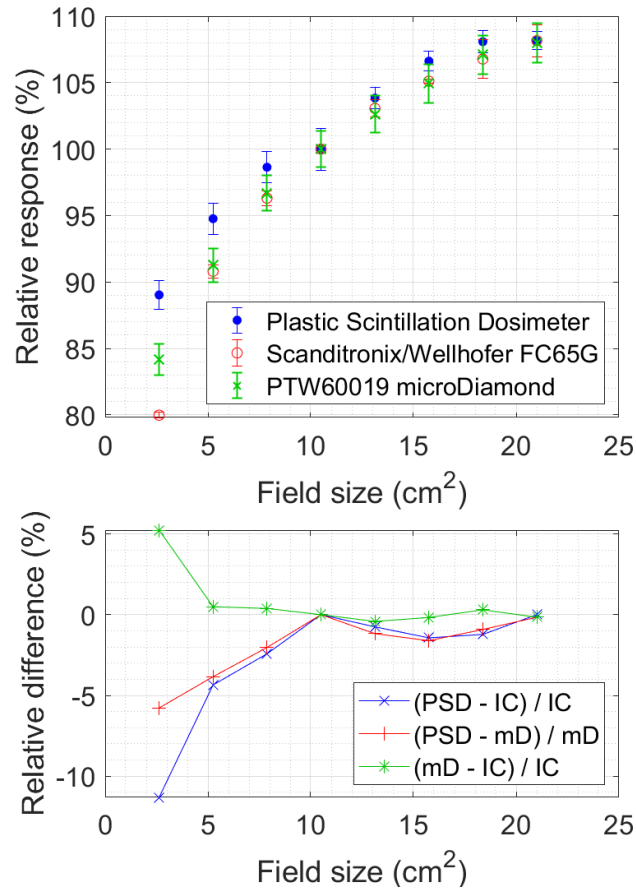


Figure 3: Output factor at 10 cm depth (top) using the in-house plastic scintillation dosimeter, ionisation chamber (FC65-G by Scanditronix / Wellhofer) and a microdiamond detector (60019 by PTW). Relative difference plot (bottom) between the output factors at 10 cm depth for ionisation chamber and PSD, and the microDiamond detector and PSD. Nominal field size is the field size at isocentre. Error bars are the combined error of each mean output factor. In the relative difference plot IC, PSD and mD are the ionisation chamber, plastic scintillation dosimeter and microDiamond detector measured output factors.

MLC defined output factors were measured with the ionisation chamber,

microDiamond detector and the PSD at depths of 10 cm and 20 cm, plotted in Figure 3 and 4, respectively. For the MLC defined output factor at 10 cm depth, the ionisation chamber and microDiamond detector at field sizes of $5.2 \times 5.2 \text{ cm}^2$ and greater. With errors taken into account, the PSD remains in agreement with the ionisation chamber at all field sizes for the 10 cm depth output factor. The PSD agreed with the microDiamond detector (within error) for all field sizes except the $2.6 \times 2.6 \text{ cm}^2$ field size.

Relative differences were calculated by taking the difference between two detectors output factors and normalising this difference to one of the reference detectors output factors. These relative differences in output factors at 10 cm depth, presented in Figure 3, possess no trend as a function of field size, suggesting that the variations between the three dosimeters are responsible for the differences. The magnitude of differences with the PSD are much larger than the difference between the ionisation chamber and the microDiamond detector, with the trendless variation suggesting that these differences arose with statistical variations of the PSDs measured responses. The observed increased response of the PSD at the $18.4 \times 18.4 \text{ cm}^2$ field size arose as a result of statistical variation.

For the output factors at 20 cm depth, the PSD was in the acceptable range of agreement, (within error) with the ionisation chamber at all field sizes except the $5.3 \times 5.3 \text{ cm}^2$ field size. The non-standard shape of the measured output factors for both depths was attributed to the LINACs MLC field shaping; for MLC field shaping, there are no changes in the backscattering from the LINACs jaws into the LINACs monitor chamber, giving the presented output factors their non-standard shape. Similar trends for MLC defined output factors are observed in Klein *et al.* [30].

A percent depth dose distribution was measured with all three dosimeters, shown in Figure 5. Electron contamination from the LINAC is focused by an MRI-LINACs fringe field; for strong fringe fields like that at the Australian MRI-LINAC, this effect makes contaminant electrons deposit high doses at shallow depths in a narrow focal spot [4]. The normalisation depth for the presented

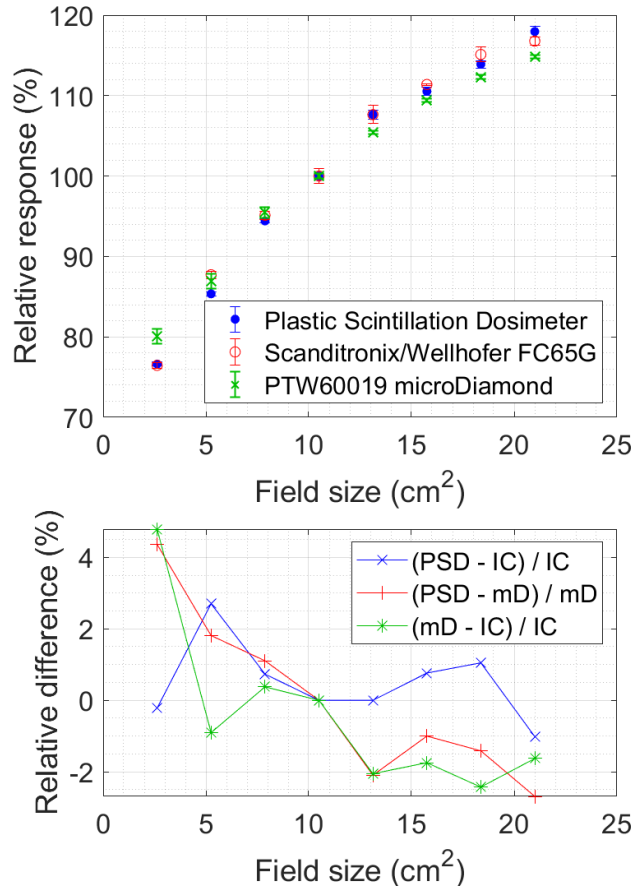


Figure 4: Output factor at 20 cm (top) and relative difference plot (bottom) as in Figure 3. Error bars and nominal field size are as described in Figure 3. IC, PSD and mD are as described for the relative difference plot in the caption for Figure 3.

PDD was chosen to be 50 mm instead of normalising the PDD to the response at 15 mm where electron contamination may be present. The microDiamond detector and ionisation chamber agreed (within error) at all depths except the 15 mm depth, where the differences in relative dose calculated between the microDiamond detector and ionisation chamber were of significantly smaller magnitude than the differences calculated with the PSD. The PSD remained in agreement (with error) with the ionisation chamber except at the 15 mm depth.

The beam quality index $TPR_{20/10}$ was measured at a field size of $10.5 \times$

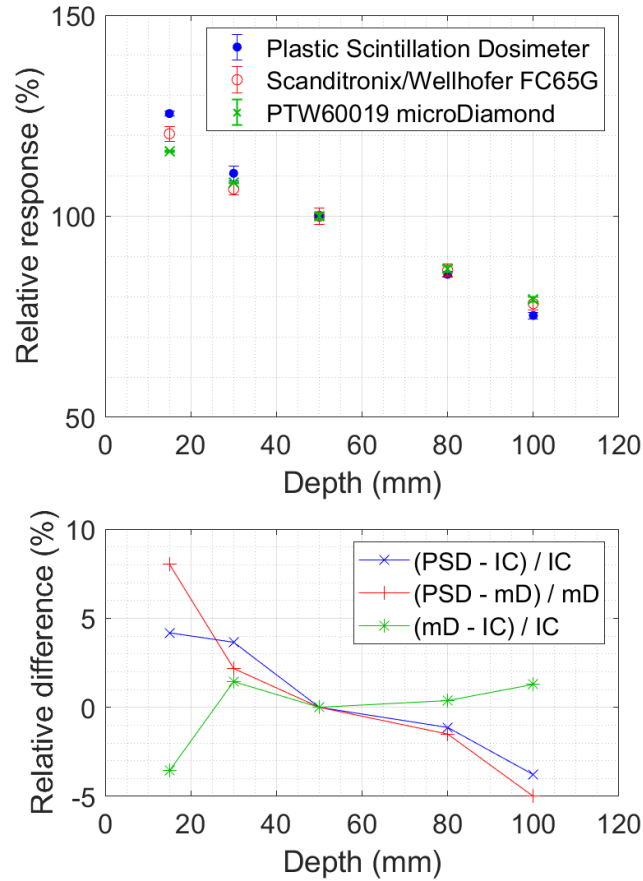


Figure 5: PDD (top) measured at the $10.5 \times 10.5 \text{ cm}^2$ field size and SSD of 2.469 m and relative difference plot between the PDDs for each detector (bottom). The PDD was normalised to the response at 50 mm depth. Error bars are the combined error of each mean PDD measurement as in Figure 3. IC, PSD and mD are as described for the relative difference plot in the caption for Figure 3.

10.5 cm^2 at the source-isocentre distance of 2.469 m. $\text{TPR}_{20/10}$ was obtained by measuring the response of the PSD at 10 cm depth and at 20 cm depth in solid water, with $\text{TPR}_{20/10}$ calculated by taking the mean of the responses at 20 cm depth and dividing by the mean of the responses at 10 cm depth. $\text{TPR}_{20/10}$ was measured to be $0.617 \pm 0.013\%$ by the PSD, while the ionisation chamber $\text{TPR}_{20/10}$ was measured to be $0.633 \pm 0.011\%$.

4. Discussion

In Figure 3, the disagreement between each detectors output factors at the smallest field size are attributed to multiple effects. The ionisation chamber had a total length and effective resolution of 2 cm; volume averaging potentially causes a reduction in the ionisation chamber response at the smallest field size. At the smallest field size: $2.6 \times 2.6 \text{ cm}^2$, detector misalignment from the centre of field position may lead to a reduction in the dose delivered to the detector [30]; each detector was aligned to isocentre with in-plane and cross-plane lasers by eye.

The electron focusing effect is known to produce a narrow lateral focal spot of electron contamination along the central axis of the photon beam [4]. Lateral volume averaging across the narrow focal spot may be a potential cause for the disagreements between each of the three detectors at the 15 mm depth. However, the alignment of each detector to the centre of the field was made by eye using the in-plane and cross-plane lasers, hence reliable positioning relative to the focal spot cannot be guaranteed. The ionisation chambers lateral resolution was 6.2 mm, with lateral volume averaging across the centre of focal spot likely to occur with the 6.2 mm lateral resolution. The PSD and microDiamond detector were orientated so they had an approximate lateral resolutions of 2.2 mm and 0.8 mm, respectively. Due to their high lateral resolutions, it is uncertain if the microDiamond and PSD were positioned at the centre of the focal spot of the electron contamination. As a result, the three detectors responses are potentially uncertain at the 15 mm depth.

As the trajectories of charged particles are altered with the presence of a magnetic field, dosimeters with a directionally independent response are desirable for MRI-LINAC dosimetry. PSDs are known to possess a directionally independent response. The ionisation chamber and microDiamond detector have been reported to possess directionally dependent responses when applied for dosimetry with perpendicular orientation MRI-LINACs [31, 32]. However, the reported directional dependences of each detector are expected to be neg-

ligible in the conditions where they were applied. For relative dosimetry with an MRI-LINAC, the ionisation chamber does not require correction for its directional dependence as any correction factor applied cancels out with itself [31]. For the perpendicular MRI-LINAC setup, the directional dependence of microDiamond reported by Woodings *et al.* [32] was 0.6% for a 0° beam angle. All measurements presented were made at the 0° beam angle, however an in-line MRI-LINAC setup was used for the presented measurements. The in-line MRI-LINAC setup used for the presented measurements was expected to reduce the magnitude of the microDiamond detectors directional dependence that was reported by Woodings *et al.* [32]. For the measurements made, the ionisation chamber and microDiamond detector are expected to be suitable references for the PSD.

From all presented relative differences in Figures 3-5, the mean difference in dose was 1.2% between the PSD and ionisation chamber, 1.9% between the PSD and microDiamond detector and 1.3% between the microDiamond detector and the ionisation chamber. The overall standard deviation of the PSD was calculated by using the relative variations in the data from all experiments presented. The 95% confidence interval in the PSD was calculated to be 1.9%, corresponding to two standard deviations in the PSDs relative response. The corresponding 95% confidence interval in the microDiamond detectors response was calculated to be 1.8%, while the corresponding confidence interval for the ionisation chambers response was calculated to be 1.9%. The similar magnitudes in the mean differences in dose and confidence intervals for each detector suggest that the in-house PSD is as effective as the ionisation chamber and microDiamond detector.

5. Conclusion

An in-house PSD was used for the measurement of output factors, a PDD and $\text{TPR}_{20/10}$ at the Australian MRI-LINAC. The PSD was evaluated by comparing the measured distributions with those measured by an ionisation cham-

ber (FC65-G, Scanditronix / Wellhofer) and a microdiamond detector (PTW 60019). Relative differences were calculated between the three detectors, where the mean difference in dose was 1.2% between the PSD and ionisation chamber, 1.9% between the PSD and microDiamond detector and 1.3% between the microDiamond detector and the ionisation chamber. The reproducibility of each dosimeter relative response was calculated and the 95% confidence interval in the PSD, ionisation chamber and microdiamond were calculated to be 1.9%, 1.9% and 1.8%, respectively. The closeness between the three mean differences in dose and 95% confidence intervals suggests that the PSD was as viable as the ionisation chamber and microDiamond detector for relative dosimetry with an MRI-LINAC. As PSDs are known to possess irradiation angle independence and magnetic field insensitivity, the presented results supports that PSDs are effective for relative dosimetry with MRI-LINAC.

6. Acknowledgements

I'd like to thank Prof. Michael Lerch for sharing the PTW60019 microDiamond presented in this paper. I'd like to thank Marco Petasecca for sharing the diode triggering system. Australian MRI-linac program is supported by the Australian NHMRC Research Council Program Grant APP1132471. This research has been conducted with the support of the Australian Government Research Training Program Scholarship. This research has been conducted with scholarship support from the South West Sydney Liverpool Health District.

References

- [1] G. Liney, B. Whelan, B. Oborn, M. Barton, P. Keall, Mri-linear accelerator radiotherapy systems, *Clinical Oncology* 30 (11) (2018) 686 – 691.
- [2] B. W. Raaymakers, A. J. E. Raaijmakers, A. N. T. J. Kotte, D. Jette, J. J. W. Lagendijk, Integrating a MRI scanner with a 6 MV radiotherapy accelerator: dose deposition in a transverse magnetic field, *Physics in Medicine and Biology* 49 (17) (2004) 4109–4118.

- [3] A. J. E. Raaijmakers, B. W. Raaymakers, J. J. W. Lagendijk, Integrating a MRI scanner with a 6 MV radiotherapy accelerator: dose increase at tissue–air interfaces in a lateral magnetic field due to returning electrons, *Physics in Medicine and Biology* 50 (7) (2005) 1363–1376.
- [4] G. P. Liney, B. Dong, J. Begg, P. Vial, K. Zhang, F. Lee, A. Walker, R. Rai, T. Causer, S. J. Alnaghy, B. M. Oborn, L. Holloway, P. Metcalfe, M. Barton, S. Crozier, P. Keall, Technical note: Experimental results from a prototype high-field inline mri-linac, *Medical Physics* 43 (9) (2016) 5188–5194.
- [5] J. Begg, A. George, S. J. Alnaghy, T. Causer, T. Alharthi, L. Glaubes, B. Dong, G. Goozee, G. Liney, L. Holloway, P. Keall, The australian MRI-linac program: measuring profiles and PDD in a horizontal beam, *Journal of Physics: Conference Series* 777 (2017) 012035.
- [6] D. J. O’Brien, D. A. Roberts, G. S. Ibbott, G. O. Sawakuchi, Reference dosimetry in magnetic fields: formalism and ionization chamber correction factors, *Medical Physics* 43 (8Part1) (2016) 4915–4927.
- [7] J. Agnew, F. O’Grady, R. Young, S. Duane, G. J. Budgell, Quantification of static magnetic field effects on radiotherapy ionization chambers, *Physics in Medicine and Biology* 62 (5) (2017) 1731–1743.
- [8] S. Stefanowicz, H. Latzel, L. Lindvold, C. Andersen, O. Jkel, S. Greilich, Dosimetry in clinical static magnetic fields using plastic scintillation detectors, *Radiation Measurements* 56 (2013) 357 – 360, proceedings of the 8th International Conference on Luminescent Detectors and Transformers of Ionizing Radiation (LUMDETR 2012).
- [9] F. Therriault-Proulx, Z. Wen, G. Ibbott, S. Beddar, Effect of magnetic field strength on plastic scintillation detector response, *Radiation Measurements* 116 (2018) 10 – 13.

- [10] L. de Prez, J. de Pooter, B. Jansen, S. Woodings, J. Wolthaus, B. van Asselen, T. van Soest, J. Kok, B. Raaymakers, Commissioning of a water calorimeter as a primary standard for absorbed dose to water in magnetic fields, *Physics in Medicine & Biology* 64 (3) (2019) 035013.
- [11] A. S. Beddar, T. R. Mackie, F. H. Attix, Water-equivalent plastic scintillation detectors for high-energy beam dosimetry: I. physical characteristics and theoretical considerations, *Physics in Medicine and Biology* 37 (10) (1992) 1883–1900.
- [12] M. A. Clift, R. A. Sutton, D. V. Webb, Water equivalence of plastic organic scintillators in megavoltage radiotherapy bremsstrahlung beams, *Physics in Medicine and Biology* 45 (7) (2000) 1885–1895.
- [13] L. L. W. Wang, D. Klein, A. S. Beddar, Monte carlo study of the energy and angular dependence of the response of plastic scintillation detectors in photon beams, *Medical Physics* 37 (10) (2010) 5279–5286.
- [14] P. Carrasco, N. Jornet, O. Jordi, M. Lizondo, A. Latorre-Musoll, T. Eudaldo, A. Ruiz, M. Ribas, Characterization of the exradin w1 scintillator for use in radiotherapy, *Medical Physics* 42 (1) (2015) 297–304.
- [15] A. Dimitriadis, I. S. Patallo, I. Billas, S. Duane, A. Nisbet, C. Clark, Characterisation of a plastic scintillation detector to be used in a multicentre stereotactic radiosurgery dosimetry audit, *Radiation Physics and Chemistry* 140 (2017) 373 – 378, 2nd International Conference on Dosimetry and its Applications (ICDA-2) University of Surrey, Guildford, United Kingdom, 3-8 July 2016.
- [16] A. Beierholm, C. Behrens, C. Andersen, Dosimetric characterization of the exradin w1 plastic scintillator detector through comparison with an in-house developed scintillator system, *Radiation Measurements* 69 (2014) 50 – 56.

- [17] J. Archer, E. Li, M. Petasecca, A. Stevenson, J. Livingstone, A. Dipuglia, J. Davis, A. Rosenfeld, M. Lerch, Synchrotron X-ray microbeam dosimetry with a 20 micrometre resolution scintillator fibre-optic dosimeter, *Journal of Synchrotron Radiation* 25 (3) (2018) 826–832.
- [18] J. Archer, E. Li, J. Davis, M. Cameron, A. Rosenfeld, M. Lerch, High spatial resolution scintillator dosimetry of synchrotron microbeams, *Scientific Reports* 9 (6873) (2019) 1–7.
- [19] L. Beaulieu, S. A. Beddar, Review of plastic and liquid scintillation dosimetry for photon, electron, and proton therapy., *Physics in medicine and biology* 61 20 (2016) R305–R343.
- [20] P. Mancosu, M. Pasquino, G. Reggiori, L. Masi, S. Russo, M. Stasi, Dosimetric characterization of small fields using a plastic scintillator detector: A large multicenter study, *Physica Medica* 41 (2017) 33 – 38.
- [21] B. Casar, E. Gershkevitch, I. Mendez, S. Jurkovi, M. S. Huq, A novel method for the determination of field output factors and output correction factors for small static fields for six diodes and a microdiamond detector in megavoltage photon beams, *Medical Physics* 46 (2) (2019) 944–963.
- [22] L. K. Webb, E. K. Inness, P. H. Charles, A comparative study of three small-field detectors for patient specific stereotactic arc dosimetry, *Australasian Physical & Engineering Sciences in Medicine* 41 (1) (2018) 217–223.
- [23] F. Therriault-Proulx, L. Beaulieu, S. Beddar, Validation of plastic scintillation detectors for applications in low-dose-rate brachytherapy, *Brachytherapy* 16 (4) (2017) 903 – 909.
- [24] M. D. Belley, O. Craciunescu, Z. Chang, B. W. Langloss, I. N. Stanton, T. T. Yoshizumi, M. J. Therien, J. P. Chino, Real-time dose-rate monitoring with gynecologic brachytherapy: Results of an initial clinical trial, *Brachytherapy* 17 (6) (2018) 1023 – 1029.

- [25] T. T. Monajemi, E. A. Ruiz, Application of plastic scintillating fibres to surface dosimetry in megavoltage photon and electron beams: considerations for cerenkov correction, *Physics in Medicine & Biology* 63 (18) (2018) 185003.
- [26] L. Archambault, A. S. Beddar, L. Gingras, R. Roy, L. Beaulieu, Measurement accuracy and cerenkov removal for high performance, high spatial resolution scintillation dosimetry, *Medical Physics* 33 (1) (2006) 128–135.
- [27] J. Archer, L. Madden, E. Li, D. Wilkinson, A. B. Rosenfeld, An algorithmic approach to single-probe cerenkov removal in pulsed x-ray beams, *Medical Physics* 46 (4) 1833–1839.
- [28] L. Madden, J. Archer, E. Li, D. Wilkinson, A. Rosenfeld, Temporal separation of cerenkov radiation and scintillation using artificial neural networks in clinical linacs, *Physica Medica* 54 (2018) 131 – 136.
- [29] L. Madden, J. Archer, E. Li, D. Wilkinson, A. Rosenfeld, Temporal separation of cerenkov radiation and scintillation using a clinical LINAC and artificial intelligence, *Physics in Medicine & Biology* 63 (22) (2018) 225004.
- [30] D. M. Klein, R. C. Taylor, L. Archambault, L. Wang, F. Therriault-Proulx, A. S. Beddar, Measuring output factors of small fields formed by collimator jaws and multileaf collimator using plastic scintillation detectors, *Medical Physics* 37 (10) (2010) 5541–5549.
- [31] S. Pojtinger, O. S. Dohm, R.-P. Kapsch, D. Thorwarth, Ionization chamber correction factors for MR-linacs, *Physics in Medicine & Biology* 63 (11) (2018) 11NT03.
- [32] S. J. Woodings, J. W. H. Wolthaus, B. van Asselen, J. H. W. de Vries, J. G. M. Kok, J. J. W. Lagendijk, B. W. Raaymakers, Performance of a PTW 60019 microDiamond detector in a 1.5 t MRI-linac, *Physics in Medicine & Biology* 63 (5) (2018) 05NT04.